2021

Experimental Confirmation Of Improvement Of Microchannel Condensers By Extraction Circuitry Using R134a

Jun Li
ACRC, the University of Illinois, Urbana, Illinois, USA, junli9@illinois.edu

Vladimir Munćan
ACRC, the University of Illinois, Urbana, Illinois, USA

Dandong Wang
ACRC, the University of Illinois, Urbana, Illinois, USA

Pega Hrnjak
ACRC, the University of Illinois, Urbana, Illinois, USA

Experimental Confirmation of Improvement of Microchannel Condensers by Extraction Circuitry Using R134a

Jun Li[1], Vladimir Munćan[2], Dandong Wang[1], Pega Hrnjak[1,3]*

[1]ACRC, the University of Illinois, Urbana, Illinois, USA

[2]University of Novi Sad, Novi Sad, Serbia

[3]Creative Thermal Solutions, Inc., Urbana, Illinois, USA

* Corresponding Author, pega@illinois.edu

ABSTRACT

This paper experimentally confirmed the benefits of liquid extraction in microchannel condensers. Experiments are conducted on a mobile air conditioning (MAC) system. R134a is used as the working fluid. An extraction tube with valve is added to one condenser so that it can work in two modes: the conventional mode and the extraction mode. Two types of experiments have been conducted: the heat exchanger-level test and the system-level test. In the heat exchanger-level tests, for the same inlet and outlet enthalpy on the refrigerant side, the extraction mode generates more condensate than the conventional mode. The extraction mode also lowers the refrigerant outlet enthalpy compared to the conventional baseline at the same refrigerant flow rate. The effects of air-side conditions have also been explored. In the system-level test, the air conditioning system with the extraction-mode condenser achieves a higher COP than the baseline under the same superheat and refrigerating cooling capacity.

1. INTRODUCTION

During flow condensation, liquid on the wall of the condenser is an extra thermal resistance reducing heat transfer. Removing the liquid phase during condensation may help to improve the condenser performance. Figure 1 presents the concept of liquid extraction in a microchannel condenser in our companion paper (Li and Hrnjak, 2021). The condenser with extraction (extraction condenser hereafter) is designed to extract liquid in the vertical second header through well-designed holes in its lower baffle to the inlet of the 4th passes. If the liquid can be drained efficiently, flow rate in downstream passes will be smaller, thus effectively reducing the pressure drop. Besides, flow at the inlet of downstream pass is close to onset of condensation, where the HTC is the highest, so the capacity for that pass may be increased. The design does not incur too much additional cost besides punching these holes in the baffle.

While Li and Hrnjak (2021) theoretically proved the improvement of a microchannel condenser by liquid extraction, the present study experimentally confirmed the improvement. The extraction condenser is the same as the one in Li and Hrnjak (2021), which is a 4-pass design with only one extraction. One condenser is modified to be able to run in

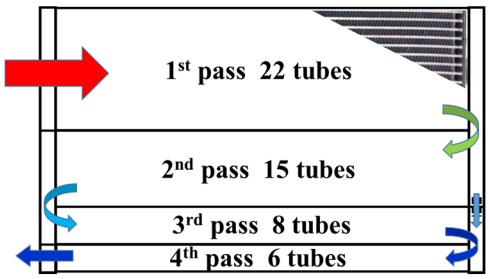

Figure 1: Extraction of liquid in a 4-pass microchannel condenser (Li and Hrnjak, 2021)

two modes: extraction and conventional, creating ease in operating the experiments. The results are provided on both the heat exchanger level and the system level.

2. FACILITY AND MEASUREMENTS

2.1 Test facility

Figure 2 illustrates the test facility for the mobile air-conditioning (MAC) system for the experiments. The system consists of an open compressor, a microchannel condenser of interest, a receiver on the high-pressure side, an electric expansion valve, and a microchannel evaporator. The compressor is an ACDelco swash-plate compressor with a fixed displacement of 165 cm^3 REV^{-1}. The evaporator is a two-slab four-pass microchannel evaporator with an overall dimension W254mm × H225mm × D39mm. It has 58 microchannel tubes in total and fin density of 10 fins per inch. The total heat transfer area on the air side is 2.87 m^2.

The condenser of interest is tested in the wind tunnel in the outdoor environmental chamber. The evaporator is installed in the wind tunnel in the indoor chamber. In both chambers, a set of PID–controlled electrical heaters are used to control the air inlet temperature for each heat exchanger. An external R404A chiller removes the heat dissipated by the condenser and the electrical heaters in the outdoor chamber.

The air flow rate is controlled by a variable-speed blower in each of the wind tunnels. The flow rate is deducted from the pressure drop and temperature at the flow nozzle downstream of a heat exchanger. The pressure drop across a flow nozzle is measured by a differential pressure transducer. The dry-bulb temperature at the nozzle outlet is measured by a Type-T thermocouple grid. In both wind tunnels, thermocouple grids are installed upstream and downstream of the evaporator and the condenser for measuring the dry-bulb temperatures. In the indoor wind tunnel, chilled-mirror dew-point sensors are also installed at the evaporator inlet and nozzle outlet. Immersed type-T thermocouples and absolute and differential pressure transducers are placed along the refrigerant circuit for depicting the refrigeration cycle. Catalog information for each component in the MAC system and the test facility can be found in Feng and Hrnjak (2015).

2.2 The condenser

Figure 3 shows the condenser setup that runs two modes for performance comparison: the conventional mode and the extraction mode. The condenser is a single-slab, cross-flow microchannel condenser. Instead of punching a hole in the lower baffle of the second header, a bypass transparent tube (extraction tube) for the 2nd and the 3rd pass is installed to simulate the extraction hole. A needle valve is installed on the extraction tube to simulate various sizes of the extraction hole. When the needle valve is shut, the flow rate in the extraction tube will be zero; the condenser is in the conventional mode (condenser in Figure 1 but without the liquid extraction). When the needle valve is open, the extraction tube allows a certain flow rate to be drained out of the second header; the condenser is in the extraction mode (condenser in Figure 1). The flow coming out of the 3rd pass will recombine with the extracted flow at the inlet

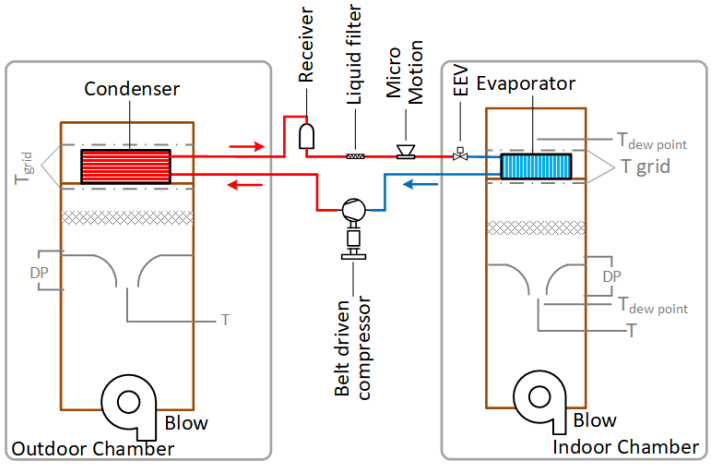

Figure 2: Schematic drawing of the A/C system test facility

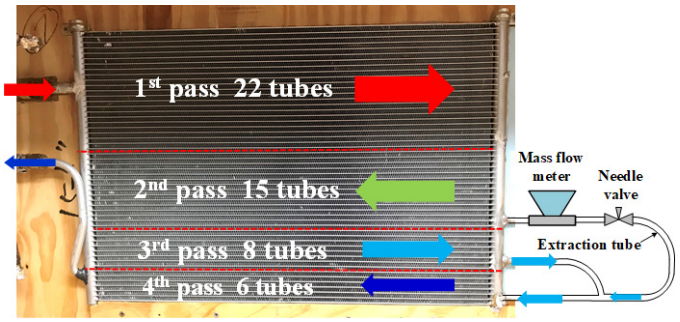

Figure 3: Condenser setup that can operate in the conventional mode and the extraction mode

to the 4th pass. A mass flow meter is installed on the extraction tube to monitor the flow rate provided that the extracted flow is in single phase.

The mass flow meter on the extraction tube is chosen to be a Coriolis-type mass flow meter. The needle valve is chosen to be for 1/4" tubes from a major valve manufacturing company. The extraction tube is chosen to be 1/4" transparent PFA tube with 1/8" inner diameter, with a total length of 2200 mm. The sizes of the needle valve and extraction tube are chosen based on 1) the pressure drop balance between the flows in the extraction tube and the 2nd pass and the 3rd pass; 2) the maximum opening allows the highest liquid flow rate from the second header to flow through at several nominal conditions.

Table 1 presents the main geometrical dimensions of the condenser. The microchannel port in one microchannel tube is estimated to have a hydraulic diameter of 0.67 mm. The number of microchannel ports per tube is 16. The photo in Figure 4 shows a cross-sectional view of multiple microchannel tubes. The drawings in Figure 4 show dimensions of one microchannel tube and one louver fin attached to the tube. The fin density of the condenser is 17 per inch, the face area 0.2447 m^2, the total air-side area 5.2895 m^2, and the total refrigerant-side area 1.3232 m^2.

2.3 Data reduction and uncertainty analysis

Capacities of both evaporator and condenser are obtained through independently measured air-side capacity and refrigerant-oil-side capacity. On the air side, the cooling capacity is calculated as Eq. (1) and the condenser capacity is calculated as Eq. (2):

$$Q_{ea} = \dot{m}_{ea,dry}\left(h_{eai} - h_{idn}\right) \tag{1}$$

$$Q_{ca} = \dot{m}_{ca,dry}\left(h_{odn} - h_{cai}\right) \tag{2}$$

where $\dot{m}_{ea,dry}$ is the dry air mass flow rate of the evaporator, h_{eai} and h_{idn} denote the evaporator air inlet and outlet enthalpies, $\dot{m}_{ca,dry}$ is the dry air mass flow rate of the condenser, and h_{cai} and h_{odn} denote the condenser air inlet and

Table 1: Main geometrical dimensions of the microchannel condenser in Figure 3

Item	Value	Item	Value
Width w. headers [mm]	620	Number of MC ports per tube [-]	16
Width w/o headers [mm]	590	Fin thickness [mm]	0.1
Width covered by fin [mm]	575	Fin pitch [mm]	1.53
Height w/ side plates [mm]	405	Louver pitch [mm]	0.77
Height w/o side plates [mm]	390	Louver length [mm]	6.0
Depth [mm]	16.3	Louver angle [-]	27
MC tube thickness [mm]	1.0	Header type	D-shape
MC tube pitch [mm]	7.8	Header equivalent diameter [mm]	18.0
MC port D_h [mm]	0.67	Length of the extraction tube [mm]	2200

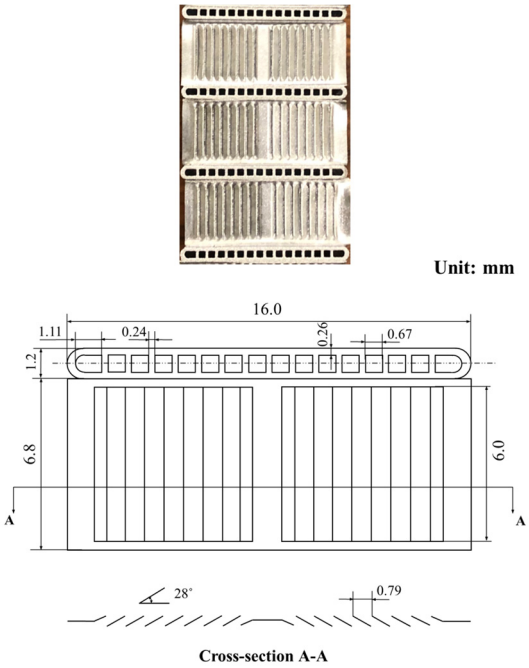

Figure 4: Dimensions of the microchannel tube and the louver fin of the condenser

outlet enthalpies. Outlet air enthalpy is determined based on temperature, pressure, and humidity at the nozzle outlet because the flow there is well mixed.

On the refrigerant-oil side, the refrigerant-oil capacity equals the product of the mass flow rate of the refrigerant-oil mixture and the specific enthalpy difference, i.e., Eq. (3) and (4). The specific enthalpy of the refrigerant-oil mixture at the evaporator inlet (h_{emi}) is assumed to be equal to that at the condenser outlet (h_{cmo}).

$$Q_{em} = \dot{m}_m \left(h_{emo} - h_{emi} \right) \tag{3}$$

$$Q_{cm} = \dot{m}_m \left(h_{cmi} - h_{cmo} \right) \tag{4}$$

In Eq. (3) and (4), $\dot{m}_m$ is the mass flow rate of the refrigerant-oil mixture, h_{emo} is the mixture specific enthalpy at the evaporator outlet, and h_{cmi} is the mixture specific enthalpy at the condenser inlet.

We assume oil is fully miscible in liquid refrigerant, and there is no heat of mixing. Refrigerant and oil are also assumed to have the same temperature and pressure on one cross-section in the pipeline. The mixture specific enthalpy (h_m) at any measurement location can be expressed as

$$h_m = \left(1 - \mathrm{OCR}\right) h_r + \mathrm{OCR}\, h_o \tag{5}$$

where h_r is the refrigerant specific enthalpy, h_o is the oil specific enthalpy, and OCR is the oil circulation ratio. h_r and h_o are then determined using the same temperature and pressure at the measurement location.

For one heat exchanger, the average of the air-side and refrigerant-oil-side capacities is taken as the final capacity:

$$Q = \frac{Q_a + Q_m}{2} \tag{6}$$

The compressor work is determined based on rotational speed v_{comp} and torque τ_{comp}:

$$W_{\text{comp}} = 2\pi \cdot \tau_{\text{comp}} \cdot \nu_{\text{comp}} \tag{7}$$

The coefficient of performance (COP) is then as:

$$\text{COP} = \frac{Q_{\text{e}}}{W_{\text{comp}}} \tag{8}$$

Using uncertainties for measured variables presented in Table 2, an uncertainty analysis of the calculated parameters is carried out in EES (2019). The uncertainties of Q of any heat exchanger and COP are ±1.5 % and ±1.75 %, respectively.

3. RESULTS AND DISCUSSION

3.1 Heat-exchanger-level comparison

For the heat-exchanger-level comparison between the extraction mode and the conventional mode, we adopt the two criteria shown in
Table **3**.

Expansion valve opening, compressor speed and evaporator air velocity are adjusted together to maintain the target constants for each criterion. For each test condition, the condenser has subcooled refrigerant at the outlet to determine the refrigerant specific enthalpy (h_{r}). Based on the thermophysical properties of refrigerants, in the superheated or the subcooled region, the specific enthalpy of a refrigerant is almost only a function of the temperature and is much less of a function of the pressure. Therefore, a lower temperature (T_{cmo}) means a lower h_{cmo}.

For Criterion 1, based on Eq. (4), the condenser with a lower T_{cmo} (h_{cmo}) has a higher capacity, thus it is more effective. For Criterion 2, based on Eq. (4) again, the condenser with a higher $\dot{m}_{\text{m}}$ has a higher capacity, thus it is more effective.

R134a is the working fluid and PAG 46 is the oil for the compressor. From tests of Criterion 1, Figure 5 shows that the extraction condenser consistently has a lower mixture outlet temperature T_{cmo} than the conventional condenser. Figure 5 demonstrates four comparisons, and the abscissa denotes the air-side condition for each comparison. While

Table 2: Uncertainties of the instruments

Measurement	**Unit**	**Uncertainty**
Refrigerant pressure	kPa	±1
Refrigerant pressure drop	kPa	±1
Air-side pressure drop	Pa	±1 %
Temperature	°C	±0.1
Refrigerant mass flow rate	g/s	±0.1
Compressor speed	-	±0.25 %
Compressor torque	N·m	±0.042

Table 3: Criteria for the heat-exchanger-level comparison between the two condenser modes

	Constants		**Parameter to compare**
	Refrigerant-oil-mixture side	**Air side**	
Criterion 1	Mass flow rate $\dot{m}_{\text{m}}$, condenser mixture inlet pressure P_{cmi}, condenser mixture inlet temperature T_{cmi}, OCR	Condenser air inlet velocity v_{cai}, condenser air inlet temperature T_{cai}, condenser air inlet relative humidity RH_{cai}	Condenser mixture outlet specific enthalpy h_{cmo}

Criterion 2	P_{cmi}, T_{cmi}, h_{cmo}, OCR	v_{cai}, T_{cai}, RH_{cai}	$\dot{m}_m$

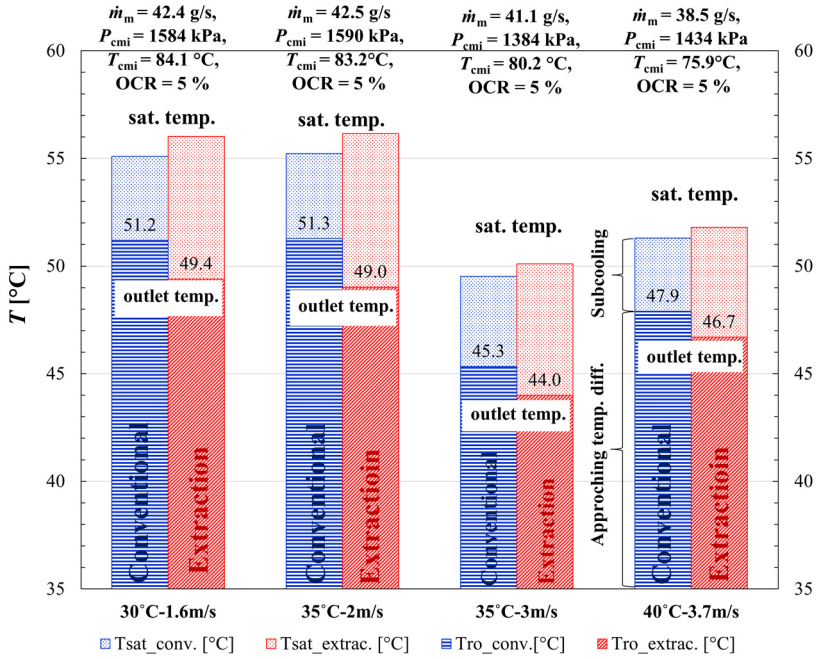

Figure 5: Refrigerant-oil mixture outlet temperature T_{cmo} (bars of the dark color) and saturation temperature T_{sat} (bars of the light color) of R134a for the two condensers at the same $\dot{m}_m$, P_{cmi}, T_{cmi}, and OCR

$\dot{m}_m$ is within the range of 40±3 g/s, the biggest difference in T_{cmo} between the two condensers is 2.3 K at the condition of 35 ˚C-2 m/s. It is worth noting that for all conditions, the saturation temperature of R134a in the extraction condenser is higher. The higher saturation temperature gives rise to a larger refrigerant-air temperature difference, constituting the main reason for capacity improvement. While the saturation temperature is calculated using the average pressure, $(P_{cmi}+P_{cmo})/2$, in the condenser, the higher saturation temperature in the extraction condenser is because of the lower pressure drop.

A bigger difference in T_{cmo} is found at low v_{cai}. It is because lower v_{cai} causes higher average refrigerant quality in the condenser thus higher pressure drop. When pressure drop is higher, the advantage of extraction to reduce the pressure drop is more significant.

For the comparisons using Criterion 2, Figure 6 shows that the extraction condenser consistently has a higher refrigerant mass flow rate than the conventional baseline. The same P_{cmi}, T_{cmi}, and T_{cmo} for the two modes are also marked in Figure 6. The improvement of R134a-oil mixture mass flow rate varies from 0.8 % to 6.2 %.

The improvement by extraction is a function of air inlet condition. Same as in Figure 5, the first three comparisons in Figure 6 demonstrate the improvement is bigger at low v_{ai}: the improvement changes from 3.7 % to 0.8 % when v_{ai} changes from 1.5 m s^{-1} to 3 m s^{-1}. From the second comparison and the fourth comparison, it also can be found that as T_{cai} becomes higher, the improvement by extraction is bigger. It is because higher T_{cai} reduces the refrigerant-air temperature difference, thus increasing the refrigerant quality in the condenser and the refrigerant-side pressure drop. When pressure drop is higher, the advantage of extraction is more significant.

3.2 System-level comparison

We use the criterion in Table 4 for the system-level tests.

For one system operating condition, test is conducted first for the condenser in the conventional mode. Then, the condenser is switched to the extraction mode with maximum opening for the extraction valve. Compressor speed is finely adjusted to match the capacity of the baseline. At the same time, the EEV opening is controlled to match the superheat with the system running with the conventional-mode condenser (conventional system hereafter). We observe

a steady liquid level in the transparent receiver downstream of the condenser in both systems.

Table 4: Criterion for the system-level comparison between the two condenser modes

Constants	Parameters to compare
System refrigerant charge Evaporator capacity Q_e Superheat at evaporator outlet SH Evaporator air side condition: v_{eai}, T_{eai}, RH_{eai} Condenser air side condition: v_{cai}, T_{cai}, RH_{cai}	Compressor speed, subcooling at condenser outlet SC, COP

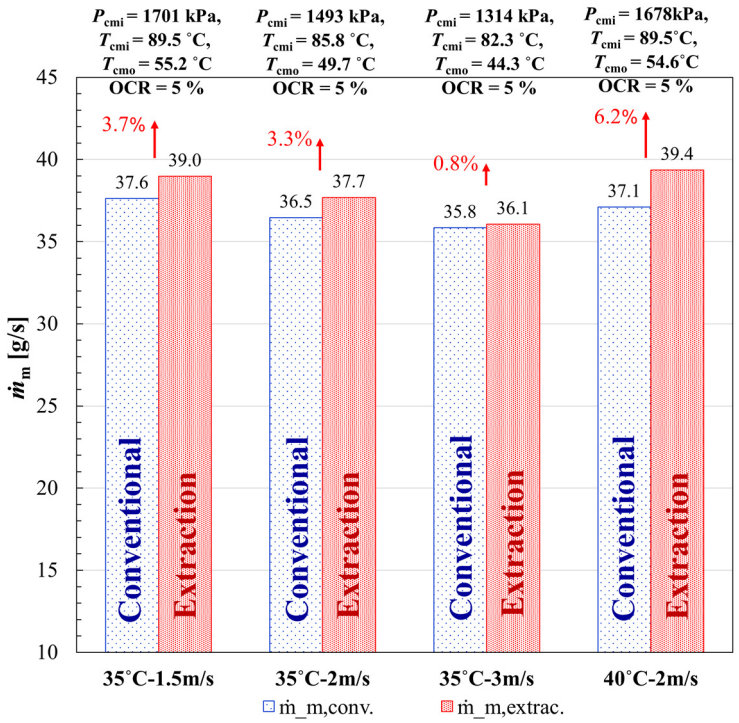

Figure 6: Mass flow rate $\dot{m}_m$ of R134a-oil mixture for the two condensers at the same P_{cmi}, T_{cmi}, T_{cmo}, and OCR

Figure 7 shows an example, condition L35a, that gives COP enhancement by the extraction condenser out of a range of test conditions. The *T-h* and *p-h* diagrams for both modes of the system are plotted in Figure 7 to identify the primary source of COP improvement. Cooling capacities are maintained at 4.28 kW with a deviation of less than ±1%.

As shown in Figure 7(a) and (b), the system with the extraction condenser (extraction system hereafter) results in 7.9 % COP increase than the system with the conventional system. The compressor speed in the extraction system is reduced by 155 rpm (8.6 %) below that of the conventional system for providing the same cooling capacity. In general, lower speed can result in higher compressor efficiencies. For the experimental result in Figure 7, isentropic efficiency (η_{isen}) in the extraction system is indeed 2.5 % higher than in the conventional system.

The mass flow rate in the extraction system is smaller because of lower by 3.2 % because of the lower compressor speed, and the difference of specific enthalpy between the evaporator outlet and inlet is larger. The reduction of condensing temperature (compressor discharge pressure) reduces the compressor work. All these effects bring a 7.9 % higher COP.

3.3 Effect of extraction valve opening

Using the same system comparison criterion shown in *Section 3.2*, Figure 8 shows the *T-h* diagrams for the system at

different valve openings on the extraction tube. The needle valve is gradually opened from 0 turn to 1 turn (0 turn corresponds to the conventional mode), since it was observed from the product catalog that the C_v value for the valve

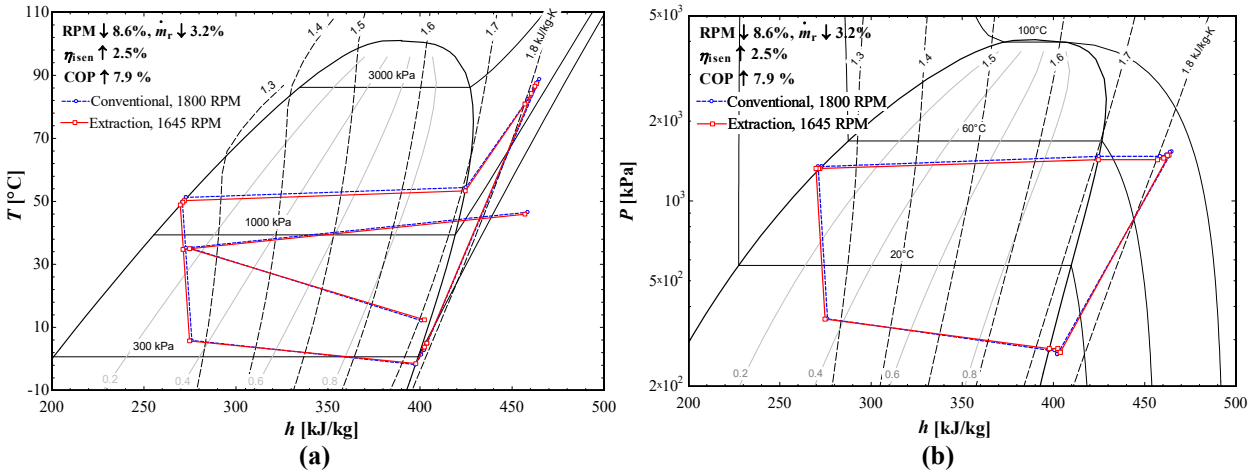

Figure 7: Comparison for the cycles with the conventional and extraction condensers at matched cooling capacity: (a) *T-h* diagram; (b) *p-h* diagram (R134a, 1700 g, T_{cai} = 35 °C, v_{cai} = 2 m/s, T_{eai} = 35 °C, $\dot{m}_{eai}$ = 11 kg/min, SH = 10 K)

has little change above 1 turn.

Table 5 lists the key parameters for the system for those different valve openings in Figure 8 (adding one more valve opening, i.e. 1 turn, in the comparison). Capacities are maintained at 4.38 kW with a deviation of less than 1%.

Figure 8 and Table 5 prove that the extraction mode outperforms the conventional mode: COP for the extraction system is higher. Because of the higher efficiency of the condenser, the condensing temperature is lower in the extraction system and the compressor speed is reduced, causing some extra benefit in the isentropic efficiency to further reduce the compressor work.

Figure 8 and Table 5 also show the COP improvement is the highest (8.6 %) at 1/2 turn. As the needle valve is open gradually from 0 turn to 1/2 turn in Figure 3, the saturation temperature of the condenser and the compressor speed (N_{cp}) both become lower, causing COP to increase. As the needle valve is opened more from 1 / 2 turn to 1 turn, ΔP_c has almost no change (96.66 kPa to 96.4 kPa). N_{cp} remains the same and the compressor work increases a bit from

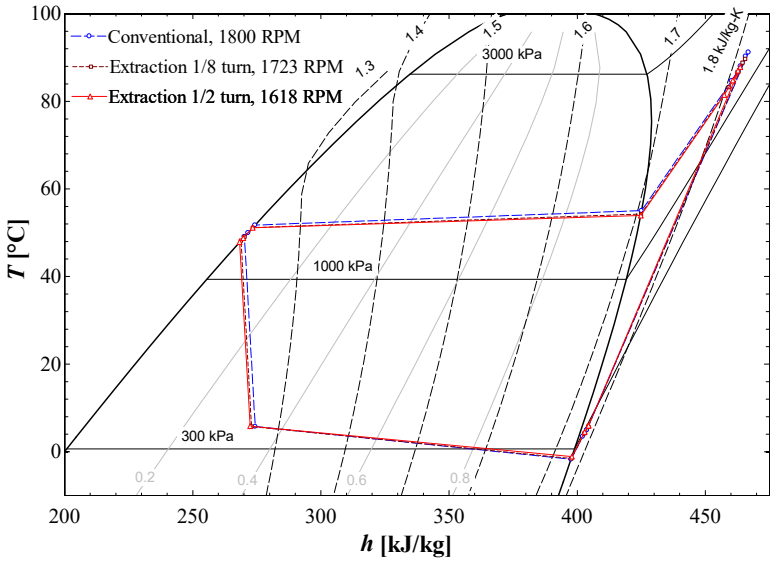

Figure 8: Effect of extraction valve opening on system performance (R134a, 1800 g, T_{cai} = 35 °C, v_{cai} = 2 m/s, T_{eai} = 35 °C, $\dot{m}_{eai}$ = 11 kg/min, SH = 10 K)

Table 5: Operating conditions for the system with the conventional condenser

	Q_e [kW]	COP	COP improvement	N_{cp} [RPM]	$\dot{m}_r$ [g/s]	ΔP_c [kPa]
Conv.	4.397	1.76	-	1800	36.56	117.1
Extrac. 1/8 turn	4.408	1.837	+4.4%	1723	36.09	108.2
Extrac. 1/4 turn	4.375	1.893	+7.5%	1644	35.61	99.63
Extrac. 1/2 turn	4.367	1.912	+8.6%	1618	35.53	96.66
Extrac. 1 turn	4.356	1.899	+7.9%	1618	35.67	96.4

2284 W to 2293 W, which causes COP to decrease a little bit.

4. SUMMARY AND CONCLUSION

The same condenser is operated in a complete automotive system, first in conventional mode, and after that with the extraction of condensate from an intermediate header. The results of the experiments confirmed that the extraction circuitry helps the condenser.

The effect of extraction is first tested on the heat exchanger level. At the same refrigerant inlet and exit temperature, a maximum increase of 6.2 % of the refrigerant mass flow rate is achieved in the extraction condenser over the conventional condenser. Using another comparison criterion, the extraction condenser lowers the refrigerant exit temperature compared to the baseline for the same refrigerant flow rate. The improvement by extraction decreases as the air inlet velocity increases and increases as the air inlet temperature increases.

Then the effect of extraction is explored in a MAC system measuring COP at matched cooling capacity. When the cooling capacity is matched by adjusting the compressor speed, the COP improvement is up to 8.6 % compared to the system with the conventional condenser. The COP improvement is the highest at one specific opening of the extraction valve.

There was no device inside of the header, and the efficiency of the separation in the header was neither measured nor observed. Authors believe that further improvements in the condenser and the system can be achieved by better separation.

NOMENCLATURE

A	heat transfer area	(m^2)
D	diameter	(m)
G	mass flux	(kg/m^2-s)
HTC	heat transfer coefficient	(W/m^2-K)
$\dot{m}$	mass flow rate	(g/s)
MAC	mobile air conditioning	
N	rotational speed	(RPM)
OCR	oil circulation ratio	(-)
P	pressure / pitch	(kPa) / (mm)
Q	capacity	(kW)
RH	relative humidity	(-)
SC	subcooling	(K)
SH	superheat	(K)
T	temperature	(°C)
UA	thermal conductance	(W/K)
v	velocity	(m/s)

W	work	(W)
x	vapor quality	(-)

Greeks

ρ	density	(kg/m^3)
τ	torque	(N m)
v	rotational speed	(rev/s)

Subscripts

c	condenser
ca	condenser air side
ca,dry	condenser dry air
cai	condenser air inlet
cmi	condenser mixture inlet
cmo	condenser mixture outlet
comp	compressor
e	evaporator
ea	evaporator air side
ea,dry	evaporator dry air
eai	evaporator air inlet
emi	evaporator mixture inlet
emo	evaporator mixture outlet
h	hydraulic
idn	indoor nozzle
L	liquid phase
m	refrigerant-oil mixture
o	oil
odn	outdoor nozzle
r	refrigerant
ri	refrigerant inlet
ro	refrigerant outlet
sat	saturation
V	vapor phase

REFERENCES

EES (2019). Engineering Equation Solver. Academic Professional Version 10.644-3D. F-Chart Software, Middleton, WI, USA.

Feng, L. & Hrnjak, P. (2015). Experimental study of reversible AC/HP system of electric vehicles. *ACRC Report TR-314*. University of Illinois, Urbana, USA.

Li, J., Muncan, V., Wang, D. & Hrnjak, P. (2021). Extraction as a way to improve the performance of microchannel condensers using R134a. *18th International Refrigeration and Air Conditioning Conference at Purdue* (Paper 210081). West Lafayette, Indiana, USA.

SAE International (2008). Procedure for Measuring System COP [Coefficient of Performance] of a Mobile Air Conditioning System on a Test Bench, SAE Surface Vehicle Standard J2765 OCT2008.

ACKNOWLEDGMENT

The authors thankfully acknowledge the financial and technical support provided by the Air Conditioning and Refrigeration Center at the University of Illinois at Urbana-Champaign and Creative Thermal Solutions, Inc.